

# Supplementary material for "Triple oxygen isotope composition of CO<sub>2</sub> in the upper troposphere and stratosphere"

Getachew Agmuas Adnew<sup>1</sup>, Gerbrand Koren<sup>2</sup>, Neha Mehendale<sup>1</sup>, Sergey Gromov<sup>3</sup>, Maarten Krol<sup>1,4</sup>, and Thomas Röckmann<sup>1</sup>

<sup>1</sup>Institute for Marine and Atmospheric research Utrecht (IMAU), Physics Department, Science Faculty, Utrecht University, Princetonplein 5, 3584 CC Utrecht, the Netherlands

<sup>2</sup>Copernicus Institute of Sustainable Development, Utrecht University, Princetonlaan 8a, 3584 CB Utrecht, the Netherlands

<sup>3</sup>Max Planck Institute for Chemistry, Hahn-Meitner-Weg 1, 55218 Mainz, Germany

<sup>4</sup>Meteorology and Air Quality, Wageningen University, Wageningen, the Netherlands

**Correspondence:** Getachew Agmuas Adnew (g.a.adnew@uu.nl)

Figure 11 in the main text uses the discrimination of assimilation against  $\Delta'^{17}O$  as established in Adnew et al. (2020) to parameterize the isoflux from assimilation. The results shown there are for a temperature of 15°C and relative humidity of 75%. Here we illustrate the dependence of the results on pressure and temperature.

$$\Delta_A \Delta'^{17}O = (\Delta'^{17}O_{UT} - \Delta'^{17}O_M) \times (-0.150 \times e^{3.707 \times \frac{c_m}{c_a}} + 0.028) \quad (S1)$$

- 5 Figure S1 shows the sensitivity of the discrimination against  $\Delta'^{17}O$  ( $\Delta_A \Delta'^{17}O$ ) to relative humidity and temperature. The value of  $\Delta_A \Delta'^{17}O$  increases with rising relative humidity but decreases with increasing temperature. Both relative humidity and temperature influence equation S1 through  $\Delta'^{17}O_M$  (see equation S2) (Adnew et al., 2020). An increase in relative humidity enlarges the difference between the three isotope slope of transpiration and the reference slope ( $\theta_{trans} - 0.528$ ), which lowers  $\Delta'^{17}O_M$ . This, in turn, raises the  $(\Delta'^{17}O_{UT} - \Delta'^{17}O_M)$  difference, leading to stronger discrimination (see Figure S1a). Conversely, when temperature increases, both  $\alpha_{CO_2-H_2O}$  and  $\alpha_{trans}$  decrease, resulting in a relatively enriched  $\Delta'^{17}O_M$  value. This reduces the  $(\Delta'^{17}O_{UT} - \Delta'^{17}O_M)$  difference and, consequently, leads to a lower discrimination (see Figure S1b).

$$\Delta'^{17}O_M = \Delta'^{17}O_{MW} + (\theta_{trans} - 0.528) \times \ln \alpha_{trans} + (\theta_{CO_2-H_2O} - 0.528) \times \ln \alpha_{CO_2-H_2O} \quad (S2)$$

- The mass balance model discussed in the main text solves for the GPP flux based on assumptions of several other parameters. Here we illustrate the dependence of this calculation on these assumptions. Figure S2 illustrates the dependence of Gross Primary Production (GPP) on the net isoflux of  $\Delta'^{17}O$  from the stratosphere to the troposphere ( $\Delta'^{17}O_{ST}$ -isoflux, panel a) and the  $\Delta'^{17}O$  value of the upper troposphere (panel b) for different  $c_m/c_a$  values (color bars in both panels). A higher net isoflux of  $\Delta'^{17}O$  to the troposphere leads to an increase in GPP to maintain the steady state assumption (see Equation 5 in the main text and Figure S2a). Conversely, a higher  $\Delta'^{17}O_{UT}$  results in a lower GPP, as it increases the  $\Delta_A \Delta'^{17}O$  value (see Figure S2b). Figure S3 illustrates the sensitivity of GPP to relative humidity and temperature, again with different  $c_m/c_a$  ratios indicated as

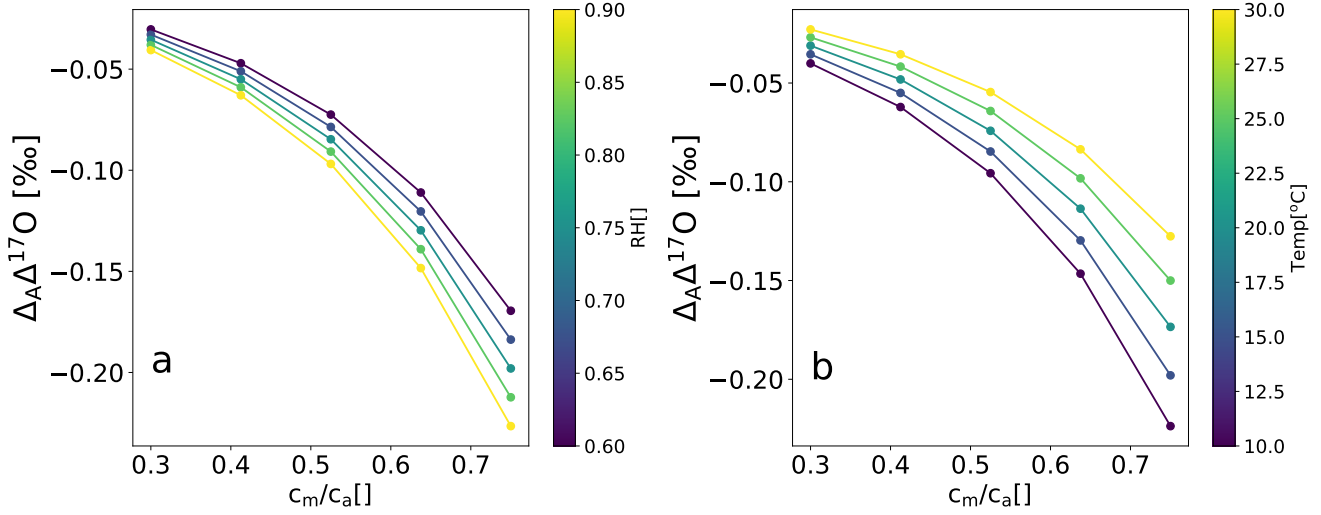


**Figure S1.** Relationship between  $c_m/c_a$  and  $\Delta_A\Delta'^{17}\text{O}$  under varying conditions of relative humidity (a) and temperature (b), based on the experiments by (Adnew et al., 2020). Relative humidity and temperature are indicated by the colour bars.

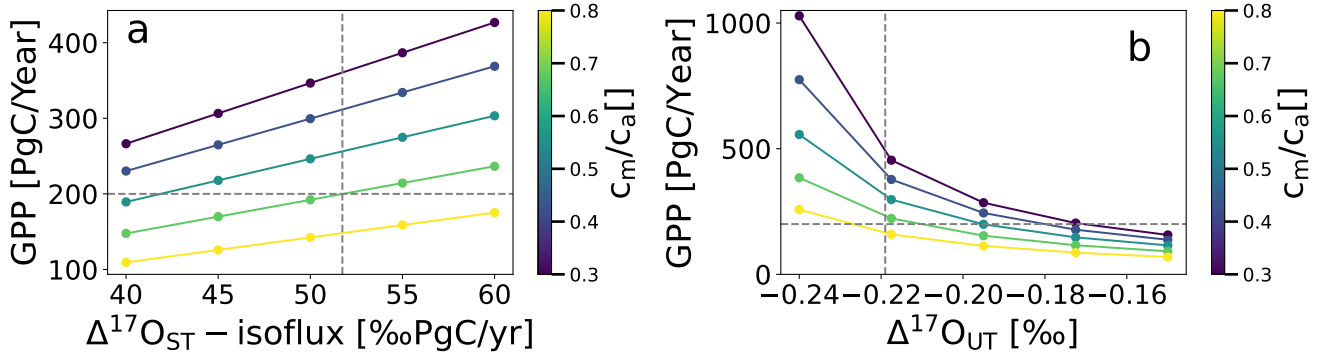


**Figure S2.** Sensitivity of GPP to the  $\Delta'^{17}\text{O}$  stratosphere-troposphere isoflux and  $\Delta'^{17}\text{O}$  value of upper troposphere. (a) The relationship between  $\Delta'^{17}\text{O}$  stratosphere-troposphere isoflux and GPP, with different  $c_m/c_a$  ratios indicated by the color bar. (b) The relationship between  $\Delta'^{17}\text{O}$  in the upper troposphere and GPP, with different  $c_m/c_a$  ratios indicated by the color bar.

20 color bars. An increase in relative humidity leads to a decrease in GPP due to an increase in  $\Delta_A\Delta'^{17}\text{O}$ . Conversely, an increase in temperature results in an increase in GPP, as higher temperatures cause a decrease in  $\Delta_A\Delta'^{17}\text{O}$ , as described above.

The  $\Delta'^{17}\text{O}$  value of  $\text{CO}_2$  equilibrated with ocean water and diffused back to the atmosphere ( $\Delta'^{17}\text{O}_o$ ) is calculated from the  $\Delta'^{17}\text{O}$  value of ocean water (OW) as  $\Delta'^{17}\text{O}_o = \Delta'^{17}\text{O}_{OW} + (\theta_{\text{CO}_2-\text{H}_2\text{O}} - 0.528) \times \ln\alpha_{\text{CO}_2-\text{H}_2\text{O}} + (\theta_{\text{diff-water}} - 0.528) \times \ln\alpha_{\text{diff-water}}$ , where  $\theta_{\text{diff-water}}$  is the oxygen triple isotope slope for  $\text{CO}_2$  diffusion in solution (water). The  $\Delta'^{17}\text{O}$  values of

**Table S1.** Information on flight numbers of the Caribic flights with the whole air sampler (WAS) from which samples were analyzed for this study, with flight dates and flight routes.

Sample	Date	Route
WAS-25	28-July-2000	Windhoek to Munich
WAS-28	18-Oct-2000	Male to Munich
WAS-29	05-Nov-2000	Male to Düsseldorf
WAS-30	03-Dec-2000	Capetown to Munich
WAS-31	19-Jan-2001	Colombo to Düsseldorf
WAS-32	01-Apr-2001	Colombo to Düsseldorf
WAS-33	14-May-2001	Holguin to Düsseldorf
WAS-34	19-May-2001	Düsseldorf to Isla Margartia
WAS-35	11-June-2001	Holguin to Düsseldorf
WAS-36	25-June-2001	Holguin to Düsseldorf
WAS-37	9-July-2001	Holguin to Düsseldorf
WAS-47	27-Apr-2002	Varadero to Düsseldorf

25 soil invasion and soil respiration are calculated from the  $\Delta^{17}O$  value of meteoric water (MW), as  $\Delta^{17}O_{SI} = \Delta^{17}O_{MW} + (\theta_{CO_2-H_2O} - 0.528)$  and  $\Delta^{17}O_R = \Delta^{17}O_{MW} + (\theta_{CO_2-H_2O} - 0.528) + (\theta_{diff-air} - 0.528) \times \ln\alpha_{diff-soil}$ .

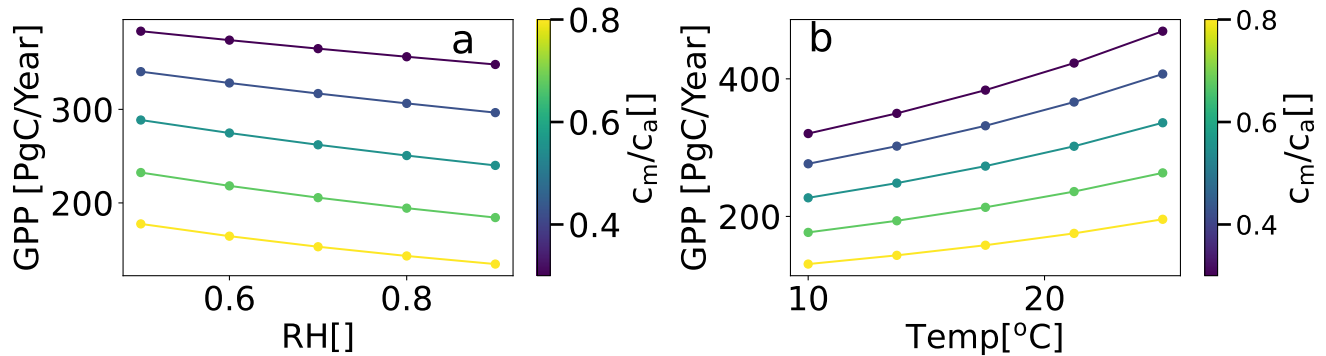


**Figure S3.** Sensitivity of GPP to relative humidity (a) and temperature (b), with different  $c_m/c_a$  ratios indicated by the color bar.

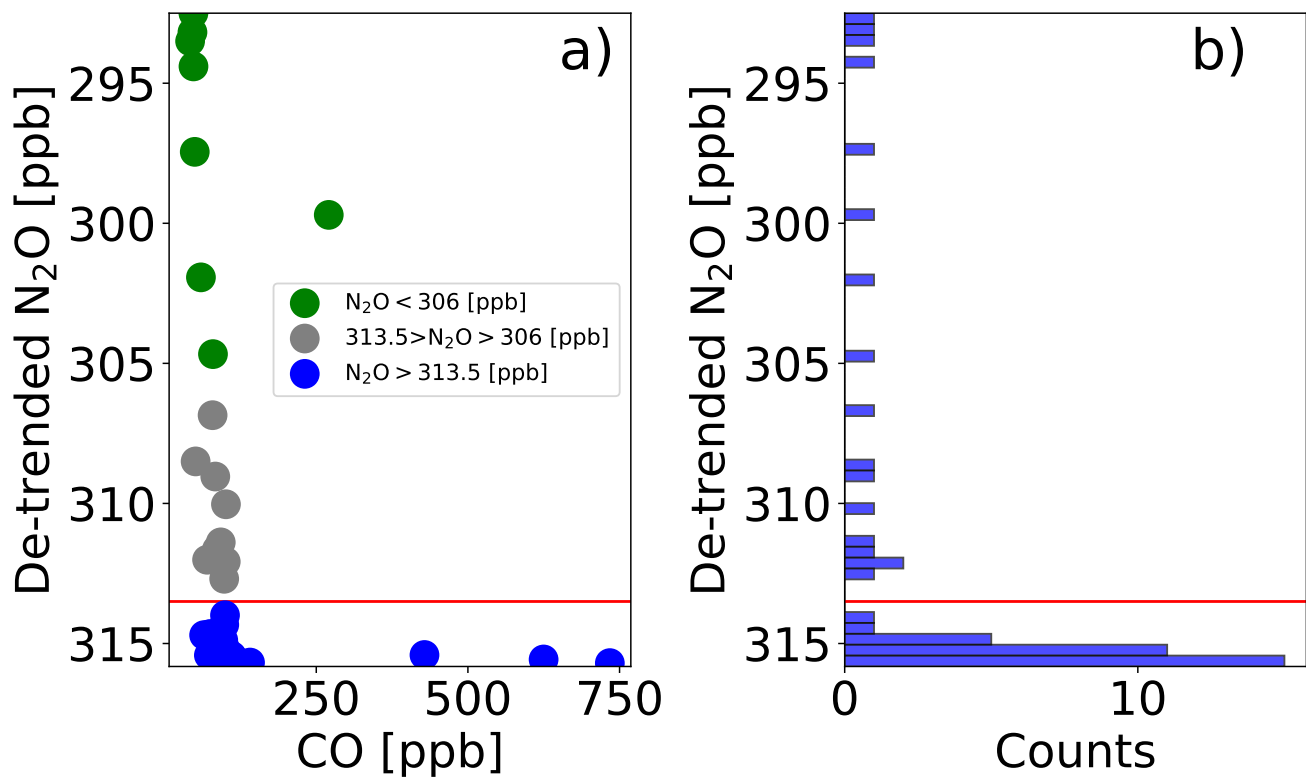


**Figure S4.** a) CARIBIC N<sub>2</sub>O data de-trended to the year 2001 versus CO. b) Histogram of CARIBIC N<sub>2</sub>O data de-trended to the year 2001. Red lines (313.5 ppb) indicate the cut-off between upper tropospheric and stratospheric air.

**Table S2.** Sampling altitude and coordinates, mole fraction of CO<sub>2</sub> and other trace gases, and the  $\delta^{13}\text{C}$ ,  $\delta^{17}\text{O}$ ,  $\delta^{18}\text{O}$ , and  $\Delta^{17}\text{O}$  values of CO<sub>2</sub> for CARIBIC samples. WAS stands for whole air sample.

Sample	Long	Lat	CH <sub>4</sub>	CO <sub>2</sub>	N <sub>2</sub> O	$\delta^{14}\text{CO}$	O <sub>3</sub>	CO	$\delta^{13}\text{C}$	$\delta^{18}\text{O}$	$\delta^{17}\text{O}$	$\Delta^{17}\text{O}$
WAS-25-1	16.01	-18.05	1751.13	368.02	314.88	8.471	60.28	96.62	-8.023	39.307	20.294	-0.266
WAS-25-2	14.49	-12.99	1744.27	368.7	314.67	8.387	62.89	73.98	-8.054	41.793	21.623	-0.226
WAS-25-3	12.91	-7.95	1744.35	368.65	314.67	61.592	65.49	75.55	-8.073	41.997	21.754	-0.201
WAS-28-1	70.13	8.72	1770.9	366.74	315.37	5.528	28.52	85.79	-7.951	40.914	21.164	-0.229
WAS-29-2	66.77	12.88	1744.97	368.03	315.01	7.652	57.94	94.99	-8.014	42.289	21.881	-0.224
WAS-30-1	18.58	-28.8	1728.63	368.59	314.7	8.565	67.73	65.13	-8.035	41.461	21.437	-0.240
WAS-30-2	17.71	-23.78	1751.8	369.03	315.29	7.062	63.57	90.08	-8.042	42.330	21.915	-0.212
WAS-30-3	16.23	-18.8	1746.11	368.48	315.3	6.694	46.17	95.75	-8.038	42.299	21.888	-0.222
WAS-30-4	14.7	-13.72	1743.99	368.42	315.13	6.879	44.82	98.83	-8.027	42.311	21.885	-0.232
WAS-30-5	13.2	-8.65	1767.5	367.76	315.43	6.931	42.94	110.1	-8.002	42.342	21.914	-0.218
WAS-30-6	11.15	-3.69	1748.38	368.81	315.41	-7.986	89.67	428.4	-8.033	42.084	21.792	-0.207
WAS-30-7	9.54	1.49	1776.6	369.77	315.68	8.129	51.37	140.8	-8.049	42.277	21.879	-0.220
WAS-30-8	9.18	7.3	1764.97	369.04	315.44	7.947	44.86	96.92	-8.034	41.837	21.661	-0.211
WAS-30-9	8.41	13.3	1759.65	369.06	315.52	7.862	55.25	95.27	-8.031	41.804	21.609	-0.244
WAS-30-10	7.88	19.14	1758.88	368.93	315.45	7.566	49.79	93.12	-8.031	41.828	21.651	-0.216
WAS-30-11	7.26	24.77	1770.74	368.58	315.17	10.169	54.73	77.49	-8.033	41.441	21.465	-0.201
WAS-30-12	6.85	30.18	1779.24	369.31	315.14	8.143	40.09	82.53	-8.077	41.284	21.377	-0.208
WAS-31-1	75.35	9.93	1763.85	369.87	315.62	7.251	27.15	95.77	-8.066	41.407	21.42	-0.229
WAS-31-2	71.15	13.34	1767.7	370.03	315.57	-8.035	113.8	624.8	-8.063	42.206	21.843	-0.220
WAS-31-3	67.04	16.52	1761.45	369.77	315.64	8.709	58.75	111.4	-8.055	42.209	21.837	-0.227
WAS-31-4	62.87	19.56	1757.4	369.61	315.61	8.126	51.62	102	-8.054	41.976	21.713	-0.230
WAS-31-10	40.79	40.41	1753.95	369.27	312.01	35.816	146.5	69.99	-8.082	41.307	21.464	-0.135
WAS-31-11	34.43	42.79	1734.7	368.31	308.5	59.519	238.8	51.1	-8.042	41.652	21.727	-0.052
WAS-32-1	74.9	10.3	1748	371.21	315.68	6.471	51.1	86.29	-8.113	41.902	21.694	-0.211
WAS-32-2	70.48	13.87	1745.58	371.01	315.52	6.55	46.73	83.49	-8.123	41.537	21.497	-0.219
WAS-32-3	66.1	17.22	1737.53	370.51	315.42	5.889	42.46	72.97	-8.097	41.967	21.715	-0.224
WAS-32-12	22.53	46.53	1756.2	371.74	312.08	26.277	136.2	100.77	-8.188	41.769	21.703	-0.135
WAS-33-1	-70.36	21.7	1750.6	373.2	315.7	-8.202	89.83	734	-8.217	41.662	21.562	-0.219
WAS-33-2	-64.63	24.14	1748.2	372.83	315.68	7.681	26.95	89.08	-8.200	41.817	21.636	-0.225
WAS-33-3	-59.14	27.34	1755.85	372.97	315.82	6.597	33.79	95.18	-8.211	41.827	21.636	-0.230
WAS-33-6	-40.34	35.8	1796.6	373.26	315.47	11.774	86.19	111.6	-8.244	42.066	21.771	-0.219
WAS-33-7	-33.58	38.68	1774.85	373.83	314.33	14.476	75.83	98.29	-8.281	41.810	21.681	-0.177
WAS-33-8	-26.6	41.13	1760.55	372.91	311.39	25.412	151.6	92.54	-8.233	41.908	21.892	-0.108
WAS-33-9	-19.64	43.11	1650.2	368.25	293.5	80.51	467.8	42.01	-8.040	41.623	22.107	0.335
WAS-33-10	-12.94	45.69	1673.15	369.12	297.45	71.902	410.6	49.67	-8.075	41.833	22.11	0.231
WAS-34-1	-0.01	51.22	1796.05	373.44	315.54	13.464	104	103.6	-8.247	41.680	21.577	-0.214
WAS-34-7	-39.81	43.02	1698.67	370.42	301.93	54.689	332.4	59.86	-8.129	41.727	21.969	0.146
WAS-34-9	-48.46	35.4	1768.8	373.61	313.99	14.607	92.11	99.54	-8.254	41.680	21.613	-0.178
WAS-35-8	-23.18	46.51	1734.97	370.57	306.85	33.555	250.9	79.08	-8.118	42.067	21.974	-0.021
WAS-35-11	3	49.04	1683.88	370.14	299.7	53.924	372.2	270.6	-8.106	42.041	22.159	0.174
WAS-36-1	-77.31	26.05	1752.5	373.26	315.28	7.49	59.43	77.71	-8.204	41.844	21.658	-0.222
WAS-36-6	-54.89	49.77	1756.8	371.35	311.64	19.566	165	86.31	-8.138	41.915	21.823	-0.091
WAS-36-8	-33.95	52.79	1742.06	370.94	309.04	26.688	208.4	83.5	-8.116	41.936	21.899	-0.028
WAS-36-9	-23.89	53.21	1644.66	368.67	292.5	68.248	474.9	47.46	-8.046	41.654	22.169	0.379
WAS-36-10	-14.2	53.1	1719.25	370.47	304.67	38.401	244.2	79.72	-8.111	41.819	21.938	0.070
WAS-37-1	-72.23	23.16	1759.8	371.46	315.38	7.669	62.36	76.7	-8.139	41.860	21.688	-0.196
WAS-37-12	0.61	51.92	1770.65	369.84	310.03	24.511	175.4	101.1	-8.097	41.952	21.882	-0.053
WAS-47-5	-57.34	36.98	1757.86	374.66	312.69	27.139	131.4	98.2	-8.252	42.030	21.872	-0.101
WAS-47-11	-10.21	49.73	1653.2	369.9	294.4	53.034	441	47.57	-8.057	41.866	22.145	0.249
WAS-47-12	-1.27	51.53	1646.6	369.73	293.18	86.573	461.7	45.88	-8.048	42.076	22.344	0.337

**Table S3.** Sampling altitude and coordinate, mole fraction of CO<sub>2</sub> and other trace gases and the  $\delta^{13}\text{C}$ ,  $\delta^{17}\text{O}$ ,  $\delta^{18}\text{O}$  and  $\Delta^{17}\text{O}$  of CO<sub>2</sub> for StratoClim samples

Sample Name	Alt[KM]	Lat	Long	N <sub>2</sub> O	O <sub>3</sub>	CH <sub>4</sub>	CO <sub>2</sub>	CO	$\delta^{13}\text{C}$	$\delta^{17}\text{O}$	$\delta^{18}\text{O}$	$\Delta^{17}\text{O}$
KL_F3_08	15.398	33.79	30.95	327.02		1907	384.75	88	-8.552	21.962	42.484	-0.244
KL-FL2-12	11.881	41.01	23.97	323.65		1832.9	402.72	51	-8.707	27.249	43.117	-0.139
KL-FL2-13	10.685	40.91	23.67	326.85		1886.6	401.62	79	-8.600	42.518	40.464	-0.267
KL-FL3-05	17.57	34.65	27.34	320.35		1818.7	405.11	33	-8.772	17.785	43.566	-0.038
KL_F3_07	17.607	33.82	29.72	317.470		1824	402.07	38	-8.766	21.917	42.072	-0.079
KL-FL3-01	14.834	36.56	22.58	317.23		1793.4	403.97	34	-8.502	18.302	42.806	0.049
KL-FL3-04	17.545	35.11	26.12	311.74		1772.9	405.62	29	-8.720	15.173	42.585	0.177
KL-FL3-03	17.545	35.58	24.89	311.5		1761	403.63	27	-8.752	14.430	42.898	0.133
KL-FL2-05	18.418	34.54	25.68	300.32	490	1723	401.61	17	-8.729	8.799	43.341	0.140
KL-FL2-11	20.009	40.34	24.95	279.24		1629	399.83	14	-8.715	7.530	44.325	0.409
KL-FL2-07	19.428	35.39	27.54	277.49	850	1622.3	399.21	16	-8.684	8.255	44.272	0.404
KL-F3-10	19.467	33.60	30.42	275.59		1635.8	400.11	21	-8.610	11.269	43.900	0.453
KL-FL2-08	19.417	36.70	27.07	268.32	1052	1584.3	398.6	20	-8.829	10.809	44.003	0.522
KL-FL2-10	19.98	39.06	25.57	260.43		1542.1	397.4	18	-8.445	9.549	43.509	0.683
KL_F3_12	20.01	34.52	27.79	255.67		1505	392.03	17	-8.527	23.133	42.101	1.095
KL-FL3-14	20.231	35.1	26.1	240.1		1493.1	397.15	17	-8.569	8.762	43.478	1.095
KT-FL4-04	17.182	29.1	81.7	330.29	131	1913		67	-8.720	36.082	42.941	-0.182
KT_FL2_04	15.5655	29.2	81.6	329.03	89	1890.7		67	-8.904	20.930	40.452	-0.224
KT-FL2-02	15.814	28.4	83.5	328.39	70	1902		67	-8.682	36.009	40.735	-0.225
KT-FL5-15	18.168	28.1	84.2	328.39	212	1872		32	-8.765	17.073	42.790	-0.154
KT-FL2-09	17.457	28.1	84.3	328.16	157	1890		59	-8.522	31.642	43.266	-0.180
KT_FL5_07	16.9725	28.6	83.0	327.880	101	1878.9		81	-8.542	21.204	41.058	-0.263
KT-FL2-05	16.958	29.2	80.9	327.2	124	1882		57	-8.896	30.281	41.541	-0.145
KT-FL2-03	16.009	28.8	82.6	327	77	1892		69	-8.719	37.268	41.990	-0.141
KT_FL3_2	16.5215	25.7	84.4	326.95	119	1880.1		57	-8.765	20.491	39.622	-0.233
KT-FL4-10	18.184	27.7	85.4	326.86	182	1859		45	-8.806	24.099	43.099	-0.188
KT_FL5_16	17.77	28.6	83.1	326.56	240	1832.3		23	-8.72	21.399	41.212	-0.134
KT-FL4-09	17.888	28.0	84.5	325.63	168	1879		50	-8.763	26.541	41.902	-0.167
KT-FL2-01	13.253	28.1	84.3	325.26	40	1892		79	-8.549	42.594	41.234	-0.179
KT_FL3_08	17.3735	21.4	79.7	322.61	145	1829.5		43	-8.764	21.518	41.315	-0.086
KT_FL3_10	19.797	22.5	79.6	282.13	771	1663		24	-8.593	12.641	42.102	0.417
KT-FL3-16	20.198	25.2	83.1	280.68	887	1645		23	-8.708	12.237	41.619	0.428
KT_FL2_16	20.271	28.3	83.9	278.38	1048	1629		17	-8.604	9.176	42.986	0.375
KT-FL3-11	20.168	23.0	80.3	277.04	929	1624		22.3	-8.632	11.817	41.434	0.464
KT_FL2_18	20.325	29.1	81.7	269.27	1061	1601		18	-8.563	9.416	41.939	0.741

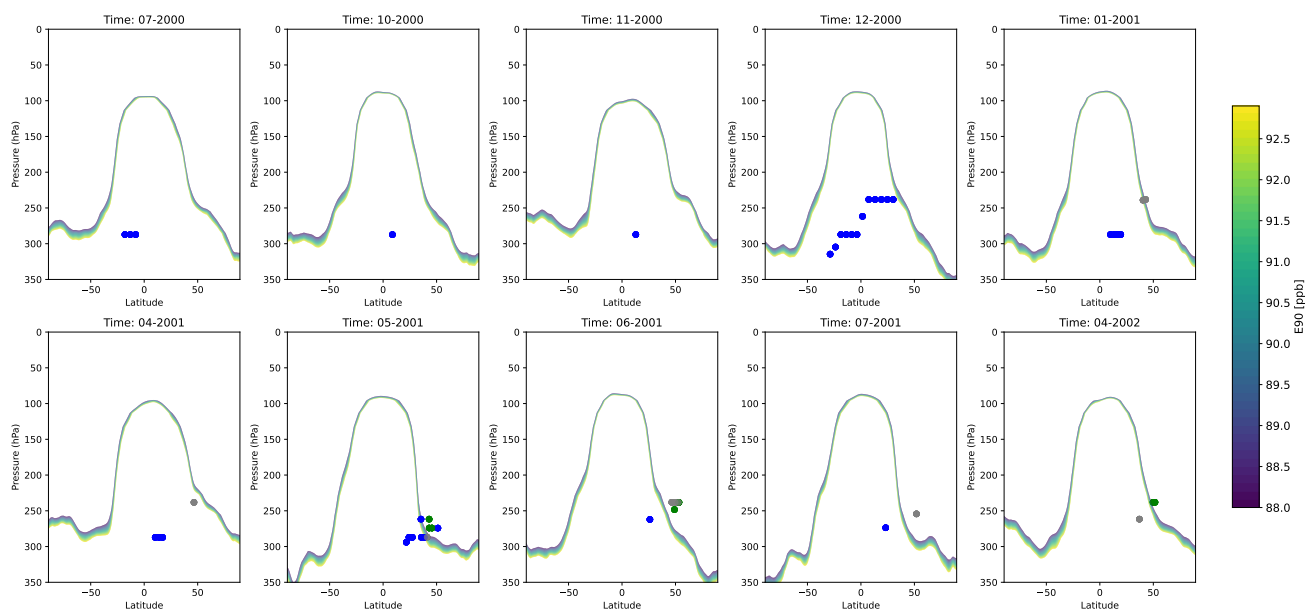


**Figure S5.** Zonal average tropopause (pressure altitude versus latitude) as modeled with the TM5 model, together with locations of the collected samples analysed in this study. The color bar specifies the artificial transport tracer E90, which is the tracer with surface emissions and an atmospheric lifetime of 90 days (E90) (Krol et al., 2018). The data points are colored in three groups based on their  $N_2O$  values, blue marker for  $N_2O \geq 313.5$  ppb, gray marker for  $313.5 > N_2O > 306$  ppb and black marker for  $N_2O < 306$  ppb.

## References

- Adnew, G. A., Pons, T. L., Koren, G., Peters, W., and Röckmann, T.: Leaf-scale quantification of the effect of photosynthetic gas exchange on  $\Delta^{17}\text{O}$  of atmospheric  $\text{CO}_2$ , *Biogeosciences Discuss.*, 2020, 1–37, <https://doi.org/10.5194/bg-2020-91>, 2020.
- 30 Krol, M., De Bruine, M., Killaars, L., Ouwersloot, H., Pozzer, A., Yin, Y., Chevallier, F., Bousquet, P., Patra, P., Belikov, D., et al.: Age of air as a diagnostic for transport timescales in global models, *Geoscientific Model Development*, 11, 3109–3130, 2018.